



ARTICLE



<https://doi.org/10.1038/s43247-020-0001-2>

OPEN

# Dynamic ice loss from the Greenland Ice Sheet driven by sustained glacier retreat

Michalea D. King<sup>1</sup>✉, Ian M. Howat<sup>1</sup>, Salvatore G. Candela<sup>1</sup>, Myoung J. Noh<sup>1</sup>, Seongu Jeong<sup>2</sup>, Brice P. Y. Noël<sup>3</sup>, Michiel R. van den Broeke<sup>3</sup>, Bert Wouters<sup>3,4</sup> & Adelaide Negrete<sup>1</sup>

The Greenland Ice Sheet is losing mass at accelerated rates in the 21st century, making it the largest single contributor to rising sea levels. Faster flow of outlet glaciers has substantially contributed to this loss, with the cause of speedup, and potential for future change, uncertain. Here we combine more than three decades of remotely sensed observational products of outlet glacier velocity, elevation, and front position changes over the full ice sheet. We compare decadal variability in discharge and calving front position and find that increased glacier discharge was due almost entirely to the retreat of glacier fronts, rather than inland ice sheet processes, with a remarkably consistent speedup of 4–5% per km of retreat across the ice sheet. We show that widespread retreat between 2000 and 2005 resulted in a step-increase in discharge and a switch to a new dynamic state of sustained mass loss that would persist even under a decline in surface melt.

<sup>1</sup>Byrd Polar and Climate Research Center & School of Earth Sciences, The Ohio State University, Columbus, OH, USA. <sup>2</sup>Department of Earth System Science, University of California Irvine, Irvine, CA, USA. <sup>3</sup>Institute for Marine and Atmospheric Research Utrecht, Utrecht University, Utrecht, The Netherlands. <sup>4</sup>Department of Geoscience and Remote Sensing, Delft University of Technology, Delft, The Netherlands. ✉email: [michaleaking@gmail.com](mailto:michaleaking@gmail.com)

The Greenland Ice Sheet (GrIS) has been losing mass for several decades<sup>1</sup> due to both increased surface meltwater runoff and ablation of marine-terminating outlet glaciers via calving and submarine melting, termed ice discharge. Total GrIS mass loss over the 1992–2018 period was due to approximately equal contributions from both terms<sup>1</sup> but with greater contribution from increased melt runoff after 2000, when mass losses accelerated<sup>2–4</sup>. Estimates of ice sheet discharge over multiple decades and at annual, or finer, resolution provide insight into the ice sheet's response to long-term climate forcing and ongoing change<sup>4,5</sup>. Seasonal and interannual variability in ice sheet dynamics are challenging to resolve prior to the year 2000 due to temporal and spatial data gaps. Here, we apply the rigorous methodology in ref. <sup>3</sup> to gain improved constraints on estimates of ice sheet discharge over three decades, including the period leading up to the onset of rapid glacier retreat and acceleration. Rates of Greenland glacier retreat have accelerated<sup>6</sup> and previous work has identified relationships between glacier speed and retreat<sup>7</sup> and glacier area<sup>8</sup> for smaller subsets of Greenland glaciers. We also then combine these data with high-resolution observations of time-varying calving front position changes and perform a GrIS-wide analysis of how these two variables relate on individual, regional, and ice sheet-wide spatial scales over the multi-decadal record. We discuss the timing of changes in retreat, thinning, and acceleration across the ice sheet, quantify the sensitivity of ice discharge to retreat, and describe the roles of both long-term changes in ice dynamics and surface mass balance in preconditioning regions of the ice sheet for rapid retreat, thinning, and accelerated discharge.

We find that GrIS-wide discharge is now ~14% greater than the rate observed during 1985–1999, following an observed step-increase during the early 2000's. Widespread glacier retreat explains nearly all (>90%) of the observed multi-decadal variability in discharge, with an observed increase in discharge of 4–5% per every weighted mean kilometer of retreat. We find that this sensitivity is proportionally consistent across different regions of the ice sheet, despite highly variable long-term trends in discharge. Following the step-increase in discharge, GrIS-wide totals have remained relatively stable at rates near 495–500 Gt yr<sup>-1</sup>, reflecting an increase that was sufficient to effectively shift the ice sheet to a state of persistent mass loss.

## Results

**Long-term changes in ice discharge and comparison with other studies.** We find a step-increase in decadal-scale ice discharge (Fig. 1a), with a ~60 Gt yr<sup>-1</sup>, or 14%, increase between 1985–1999 and 2007–2018 means. After reaching a temporally local maximum in 2005, annual  $D$  then temporarily decreased for 3 years. Following the temporary decline, discharge accelerated again at a slower pace of 2 Gt yr<sup>-2</sup> during 2008–2018, reaching a peak annual value of 502 ± 9 Gt yr<sup>-1</sup> in 2017 and 2018, or 17% above the 1980's average. The increase in mean annual  $D$  since 2008 has been mostly due to a steady increase in seasonal minimum values increasing with a trend of 3 Gt yr<sup>-2</sup> since 2007, indicating greater wintertime velocities relative to summertime maxima, most evident in the northwest (Supplementary Fig. 1) and in the most recent 3 years of the central west. The seasonal amplitude in  $D$  has also changed, increasing by nearly 50%, from a 1985–1990 average of 17 ± 6 to 25 ± 6 Gt yr<sup>-1</sup> for 2000–2018. To account for the uncertainty in  $D$  due to this temporal gap in ice thickness observations, we estimate  $D$  assuming the end member-cases of (1) all thickness change occurring in the first year, which maximizes the impact of thinning at the start of the period, and (2) all thinning occurring in the last year, which minimizes the impact until ~2000. We find that during the 1985–1999 period, estimates

of  $D$  can vary by an average 13 Gt yr<sup>-1</sup> (Fig. 1a) depending on when thinning occurred between temporally sparse elevation data (AeroDEM, ~1985 and ASTER, nominally ~2000), described in more details in the Methods section.

Discharge has increased in every region (defined in Supplementary Fig. 2) of the ice sheet since the 1980's, but with contrasting temporal variability. In the west, discharge slightly declined from 1985 to the late 1990's prior to larger increases after 2000. The central west (CW; Supplementary Fig. 1c) is dominated by Jakobshavn Isbræ, which accounted for an average of 30% of the regional discharge. Within the CW, discharge steadily increased by 27% after the initial retreat and acceleration of Jakobshavn Isbræ in 1999<sup>9</sup> to a peak in 2014 before declining 10% through 2018 due to Jakobshavn's slowdown<sup>10,11</sup>. Jakobshavn's observed slowdown was responsible for the majority (>75%) of the net decrease in  $D$  in the CW region, with only two other glaciers showing notable deceleration during this time. In the northwest (NW; Supplementary Fig. 1a), gradual increases in discharge began in the early 2000's and have since accelerated, increasing 36% by 2018. In the east, discharge was relatively stable during the 1980's and 1990's, with increases beginning in the southeast (SE; Supplementary Fig. 1d) in 2000 with the synchronous retreat and acceleration of multiple glaciers, including Helheim<sup>12,13</sup>. After increasing ~18% between 2000 and 2005, discharge in the SE then suddenly declined to within 5% above its initial [1980s mean] values, varying by 10% over the next decade with no clear trend. Pronounced acceleration did not begin in the central east (CE; Supplementary Fig. 1b) until the 2004 retreat and acceleration of its largest glacier, Kangerdlugssuaq, that caused a nearly 20% increase in annual  $D$  between 2003 and 2005. Following a decline and relative stability, another large retreat event at Kangerdlugssuaq in 2016<sup>14</sup> caused  $D$  to again rise near its 2005 maximum. We exclude discussion of regional patterns observed in the northern and southwestern regions due to small glacier sample size, but include regional discharge totals (with each of the two regions contributing, on average, ~10 Gt yr<sup>-1</sup>) in Supplementary Fig. 1e, f.

We compare our results with those presented in ref. <sup>5</sup> which is the only other study, to our knowledge, that estimates ice sheet-wide discharge at sub-annual resolution for a similar time period shown here. Our results closely agree with those of ref. <sup>5</sup> with a mean difference <4 Gt yr<sup>-1</sup> (~1%) and absolute biases of <8 Gt yr<sup>-1</sup> (Supplementary Fig. 3), and summertime estimates within 2 Gt yr<sup>-1</sup>. Larger wintertime differences are within the uncertainty expected from differences in interpolation methods (i.e., Kalman filter model used in this study and linear interpolation done in ref. <sup>5</sup>). While GrIS-wide biases are reduced by regionally compensating errors, we find that the two studies still closely agree on the regional scale, with mean temporal biases of <10% for all major drainage basins. This level of agreement is noteworthy given that the two studies use independently positioned flux gates and different velocity and elevation datasets. Our annual  $D$  estimates are also in general agreement with those from ref. <sup>4</sup> prior to 2002, but later diverge, with the estimates from ref. <sup>4</sup> exceeding ours, and those in ref. <sup>5</sup>, by >40 Gt yr<sup>-1</sup> (8%) in 2018, excluding peripheral glaciers and ice caps (Supplementary Fig. 3). We attribute this difference to the treatment of glaciers with missing bed topography data and how ice velocity is sampled, as described in the Supplementary Discussion (see also Supplementary Fig. 4).

**Decadal variability in components of ice sheet mass balance.** Combining our estimates of  $D$  with SMB from RACMO2.3p2<sup>15</sup>, including the peripheral glaciers and ice caps, gives a cumulative net loss of 4200 Gt between 1985 and 2018 (Fig. 1c). The average

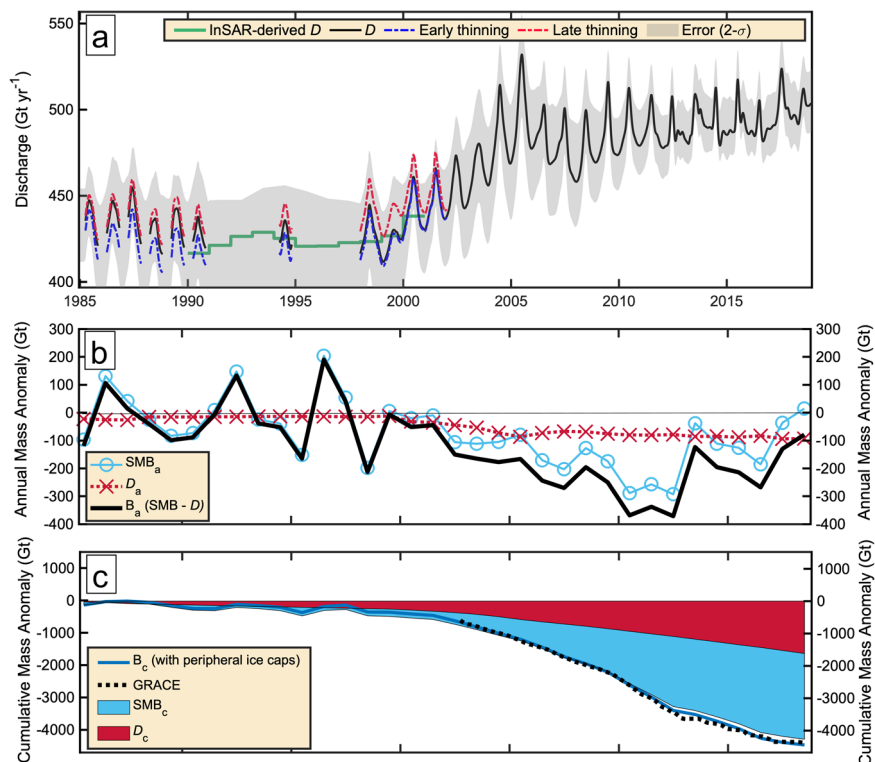


**Fig. 1 Net ice sheet discharge at contributions to total mass balance.** **a** Total GrIS discharge (black curve) with early (blue) and late-thinning (red dashes) scenarios between 1985 and 1999, and discharge estimates derived from wintertime InSAR velocities from Mouginot et al.<sup>4</sup> in green. Gray shading is  $2\text{-}\sigma$  uncertainty. **b** Net annual mass balance ( $B_a$ , black curve), annual surface mass balance ( $SMB_a$ , blue dashes with circles) and total annual discharge ( $D_a$ , red dashes with crosses). **c** Total shading shows the cumulative mass anomaly ( $B_c$ ) of  $B_a$  since 1985 broken into cumulative contributions from discharge ( $D_c$ , red) and surface mass balance ( $SMB_c$ , blue).  $B_c$  including  $SMB$  from peripheral ice caps, to match the GRACE domain, is plotted by dark blue line. GRACE estimates, updated from Wouters et al.<sup>16</sup> for the 2002–2018 time period, are also plotted on this axis as a moving 12-month average (dotted black), and shifted along the y-axis to begin at the 2002  $B_c$  value.

loss rate of  $-240 \text{ Gt yr}^{-1}$  between 2003 and 2018 is close to the approximate  $-235 \text{ Gt yr}^{-1}$  rate estimated from GRACE for the same period (update of ref. <sup>16</sup>). From 1985 to 1999, annual  $D$  consistently exceeded the mean 1961–1990 GrIS-wide  $SMB$ , typically assumed near equilibrium<sup>17,18</sup>, both with ( $424 \text{ Gt yr}^{-1}$ ) and without ( $409 \text{ Gt yr}^{-1}$ ) the inclusion of peripheral glaciers and ice caps. During this period  $SMB$  fluctuated around equilibrium, so that discharge contributed  $\sim 70\%$  to the cumulative ice sheet mass loss of  $\sim 400 \text{ Gt}$  prior to 2000 (Fig. 1c). After 1997, however,  $SMB$  anomalies became increasingly negative at a rate of nearly  $-20 \text{ Gt yr}^{-2}$  for the next 15 years, reaching approximately  $-300 \text{ Gt yr}^{-1}$  in 2012. This resulted in discharge contributing only approximately one-third of net mass losses between 2000 and 2012. Discharge has contributed to  $>50\%$  of cumulative mass losses since 2013, however, as  $SMB$  anomalies have been less negative.

For the ice sheet to gain mass, the total annual  $SMB$  must exceed the total  $D$ . Assuming the mean 1985–2000  $D$  of  $426 \pm 6 \text{ Gt yr}^{-1}$ , the mass gain from  $SMB$  offset the loss due to  $D$ , resulting in ice sheet growth, nearly 40% of the years between 1985 and 1999 (Fig. 1b), which is similar to estimated mass gain estimated in one-half of the years during the 1992–1999 period in ref. <sup>1</sup>. Increasing  $D$  to the current, post-retreat average of  $\sim 495 \text{ Gt yr}^{-1}$  cuts the percentage of years of net gain to one in five, demonstrating that the increase in discharge alone was sufficient to transition the ice sheet to a new state of persistent negative mass balance. However,  $SMB$  has also markedly declined and, assuming the post-2000 average  $SMB$ , the annual probability of net ice sheet mass gain is now only  $\sim 1\%$ . Thus, the combined

climate and dynamic states of the ice sheet are such that even a single year of mass gain is highly unlikely.

### Long-term relationships between retreat and ice discharge.

King et al.<sup>3</sup> found interannual variability in  $D$  after 2000 to be primarily associated with changes in ice front position, likely due to acceleration caused by the perturbation to the glacier stress regime during retreat<sup>19</sup>. Here we assess changes in front position and discharge since 1985, capturing the period prior to widespread retreat and acceleration. In order to compare ice front retreat and discharge, we use a subset of glaciers ( $n = 128$ ) that have continuous records of discharge and front position change. In order to assess the impact of mean front position change on the regional and ice sheet discharge and minimize the impact of small glaciers, we weight the front position of each glacier by its discharge and denote the weighted mean front position change as  $F_w$ . Figure 2a shows that GrIS  $D$  increased at an average rate of  $14 \pm 1 \text{ Gt yr}^{-1}$  per km of cumulative retreat over the 1985–2018 period, with the cumulative change in front position explaining over 93% of the change in  $D$ . This plot reveals two distinct clusters of values, before the year 2000 and after the year 2009, separated by roughly 4 km of retreat and  $50 \text{ Gt yr}^{-1}$ .  $D$  increased most rapidly during widespread acceleration and retreat between 2001 and 2005, as glaciers in the SE rapidly retreated off bathymetric highs<sup>13</sup>, at a consistent rate of  $16 \text{ Gt yr}^{-1}$  per km of cumulative retreat.  $D$  increased at a significantly lower rate of  $8 \text{ Gt yr}^{-1}$  per km of retreat following the readvance in 2006 and 2007. Since 2014, there has been little additional change in  $F_w$  or  $D$  for the ice sheet as a whole. Examining year-to-year changes in

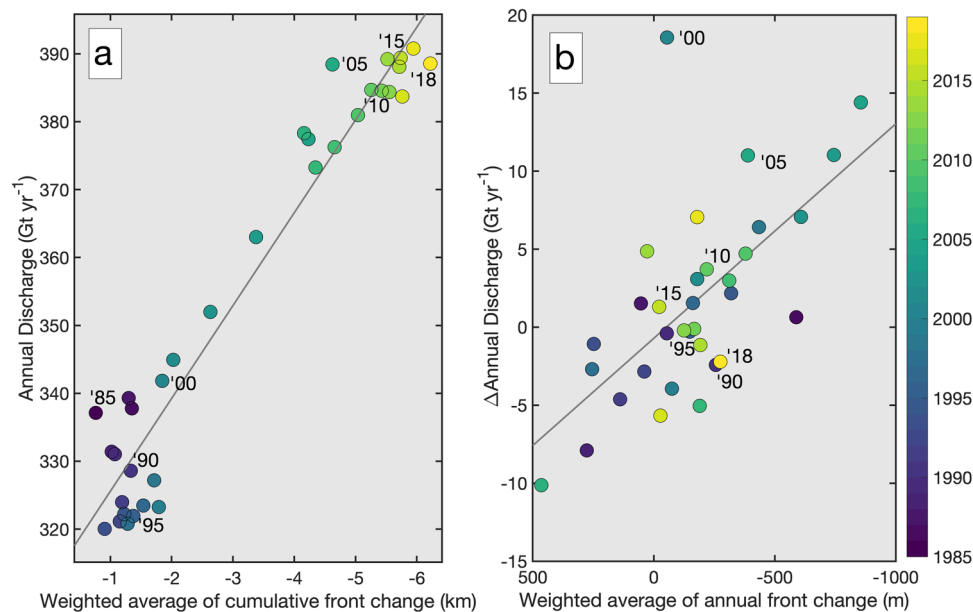


**Fig. 2 GrIS-wide relationships between discharge and front position.** **a** Annual total  $D$  versus net front position change for the 128 glaciers with continuous measurements between 1985 and 2018, with the color scale and label corresponding to the measurement year. The black line is the least-squares best fit with a slope of  $14 \text{ Gt yr}^{-1}$  per km of retreat and intercept of  $312 \text{ Gt yr}^{-1}$ . Negative front change indicates net retreat from the glacier fronts' initial position over the calendar year. Note the reversed x-axis to highlight the inverse relationship. **b** Annual changes in  $D$  and front position with labels indicating the first year (e.g., '00 is the change from 1999 to 2000). The (black line) least-squares fit has a slope of  $14 \text{ Gt yr}^{-1}$  per km of annual retreat and intercept of  $-0.7 \text{ Gt yr}^{-1}$ .

the  $F_w$  and  $D$  in Fig. 2b, we find a remarkably consistent relationship with annual changes in discharge and front position, averaging  $14 \pm 6 \text{ Gt yr}^{-1}$ , or  $\sim 4\%$ , per km of retreat, with annual variability in the front accounting for 41% of the annual variability in  $D$ . Further, we find that the change in  $D$  per km of  $F_w$  is also consistently 4–5% from region to region (Supplementary Fig. 5), indicating a similar overall sensitivity of discharge to retreat.

Since changes in discharge are dependent on changes in both ice flow speed and thickness, we would expect that, following front retreat, discharge would (i) initially increase with acceleration and then decrease due to dynamic thinning if the front restabilizes or (ii) become less sensitive to front position change if retreat continues up a prograde bed slope. While such a response is not clearly apparent for the GrIS-wide results (Fig. 2), regionally we find temporary declines in  $D$  following retreat. This is particularly evident in the SE and CE regions, where  $D$  has declined and stabilized during the recent period of relative front stability (Supplementary Fig. 5). In the NW, we find an increasing sensitivity of discharge to ubiquitous retreat, likely due to several of the actively retreating glaciers doing so on increasingly retrograde slopes, resulting in a greater increase in ice flux with retreat<sup>20–23</sup>.

The ice sheet-wide and regional sensitivities of discharge to ice front change are consistent on the scale of individual glaciers. Out of the 128 glaciers with continuous records between 1985 and 2018, nearly 70% display a significant ( $p \leq 0.05$ ) relationship between changes in discharge and front position. These glaciers account for  $\sim 75\%$  of the total  $D$ . Only 24 (19%) glaciers, accounting for 6% of  $D$ , exhibit a significant negative correlation (i.e., decreasing  $D$  with retreat) between discharge and front position. These glaciers tend to have more static fronts, varying only  $\sim 1 \text{ km}$  between 1985 and 2018, compared with 4 km for those where positive correlations are observed, and include quiescent phase surge-type glaciers and those that have retreated

along prograde bed slopes<sup>24</sup> (i.e., Upernavik Isström) during the observation period.

Retreat-driven acceleration initiates at the ice front within a distance determined by the stress coupling length (e.g., ref. 13) and then propagates up-glacier through diffusion. Therefore, the timing between retreat and changes in  $D$  may be sensitive to the location of the flux gates with respect to the ice fronts. To test this sensitivity, we repeated the above analysis using a subset of the 15 largest glaciers with dynamic flux gates positioned 2 km from the changing ice front and obtained nearly identical results, indicating that our fixed flux gates are close enough to the ice front to capture nearly instantaneous changes in front-driven dynamics. More detail regarding this analysis and an example is provided in the Supplementary Methods (see also Supplementary Fig. 6).

**Temporal patterns of thinning and retreat.** Retreat occurs through increased calving due to melting at the ice front and/or thinning of the glacier terminus toward flotation. To assess which mechanism triggered the onset GrIS-wide retreat of the late 1990's/early 2000's, we investigate the timing and magnitudes of regional retreat and thinning, weighted by discharge, as above, and plotted in Fig. 3. Between 1985 and 2000 (i.e., between the AeroDEM and start of the ASTER surface elevation datasets), glaciers thinned across their sampled flux gates by an average of 2–4% in all regions except the central west, where a 6% thinning was primarily due to the initial acceleration of Jakobshavn Isbræ in 1998–1999. During most of this initial period of thinning, ice fronts slightly advanced in the west and retreated steadily in the east since the early 1990's. The onset of rapid retreat around the year 2003/2004 was accompanied by a brief 3–4-fold increase in thinning rates in the east, abruptly ending when fronts temporarily stabilized. In contrast, thinning rates were more constant in the west, with a doubling in thinning in the NW and little



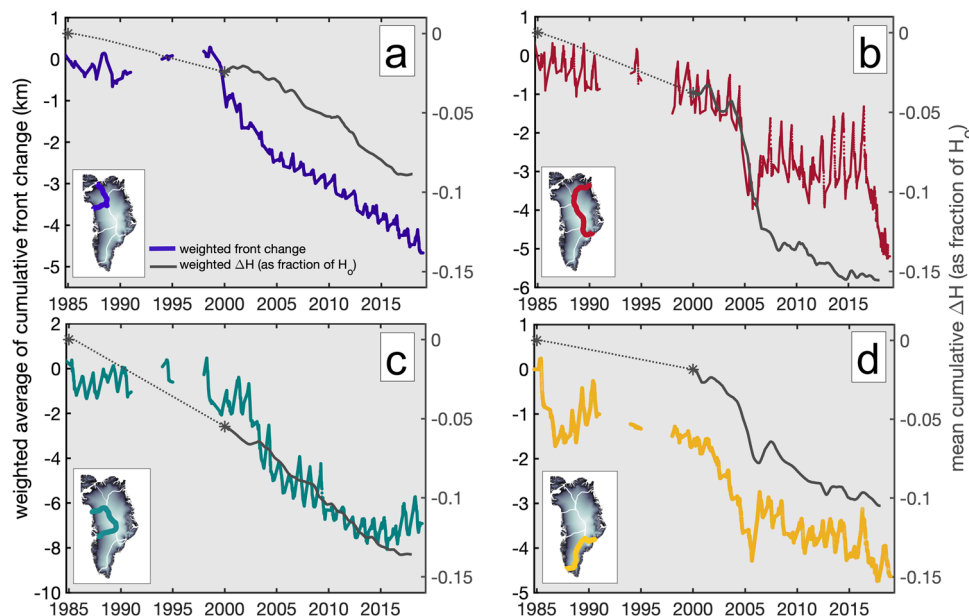


**Fig. 3 Mean regional trends in ice thickness and front position.** Net regional trends in (black curves) ice thickness and (colored curves) front position, calculated from discharge-weighted individual glacier time series in the northwest (a), central east (b), central west (c), and southeast (d), with the colors corresponding to the locations mapped in the left plane. Negative values on the left y-axis indicate net cumulative retreat over the study period. Cumulative thickness changes are shown on the right y-axes, and are calculated from the mean of all regional glaciers and expressed as fractional changes from  $H_0$ . Lighter, dotted gray lines between the two starred points indicate linear interpolation between two sparse data points, and the apparent trend during this period should be treated with caution. Please note that the limits along the left y-axes vary between panels so that time series details are more visible.

change in the CW (Fig. 3) after the onset of rapid retreat around the year 2000. We note that in the NW, the disintegration of floating ice tongues at large glaciers, as observed at Kong Oscar Glacier<sup>25</sup>, likely resulted in a delayed dynamic increase of discharge, beginning around 2003, in response to retreat (Supplementary Fig. 5). More constant thinning rates along the western margin mirrored long-term trends in retreat, which slightly decelerated after 2005 in both the NW and CW. Regional plots similar to those shown in Fig. 3 using unweighted means are shown in Supplementary Fig. 7.

Thus, in all regions, substantial thinning occurred prior to the onset of rapid retreat and acceleration in the early 2000's. To assess the potential contribution of increased surface melt to thinning, we examined changes in surface mass balance (SMB) estimated by RACMO2.3p2 relative to the 1961–1990 baseline average. We estimate thinning due to SMB anomalies along glacier flux gates, located in the ablation zone, by assuming a density of  $910 \text{ kg m}^{-3}$ . Since thinning is the sum of declining SMB and increased dynamic thinning due to ice stretching, we can estimate their relative contributions to the observed thinning for the same 1961–1990 mean reference mass balance as used above. Discharge-weighted, regional averages of thickness change due to SMB are plotted in Supplementary Fig. 8, along with the total observed thickness change and thickness change due to ice dynamics, estimated as the difference between thickness change due to SMB and the total.

Thickness changes due to SMB between 1985 and 2000 were much smaller than the observed thickness changes for all regions except the SE, where an average thinning of 8 m due to declining SMB is very close to the total observed thinning. Conversely, ice dynamics accounted for nearly all of the rapid thinning, averaging  $\sim 20 \text{ m}$ , during the episode of retreat and acceleration in the SE between 2002 and 2005. Since 2008, however, the rates of thinning due to SMB and dynamics have been nearly equal, each accounting for  $\sim 1 \text{ m yr}^{-1}$ .

Thinning due to declining SMB in the other regions began later than in the SE; the decline in SMB started in the mid-1990s in the CE, and the late 1990s in the NW and CW. In these regions, the contribution of SMB to total thinning has increased through time, reaching 30–35% in the CW and NW by 2018. Less thinning was due to SMB in the CE, accounting for <10% of the total thinning in that region by 2018.

## Discussion

We estimate over three decades of GrIS-wide ice discharge at high temporal resolution and with well-defined uncertainties, capturing a rapid, step-increase between two distinct states of discharge, and reaching an annual maximum of  $\sim 500 \text{ Gt yr}^{-1}$  in 2017 and 2018. This transition corresponds to widespread retreat of glacier calving fronts at the turn of the 21st century after a long and relatively stable period of static ice fronts on the west coast and slow retreat in the east, possibly triggered by substantial ice thinning between 1985 and 2000. In all regions except the SE, outlet glacier thinning was due, at least in part, to glacier discharge exceeding the long-term balance flux, indicating dynamic disequilibrium associated with a longer-term retreat. This is consistent with the retreat of these glaciers earlier in the 20th century<sup>26</sup>. In the SE region, thinning prior to 2000 can be primarily attributed to increased surface melt, indicating a shorter-term response to climate forcing. This agrees with the observation that the largest SE glacier, Helheim, was close to mass balance before and after its rapid retreat and temporary acceleration<sup>27</sup>. As a result of the new, semi-static rate of GrIS-wide  $D$ , that is  $>60 \text{ Gt yr}^{-1}$  higher than in 1985, annual SMB greater than two standard deviations above the 19-year (2000–2018) mean is required for the ice sheet to gain mass and is thus likely in a long-term state of persistent loss.

The overall increasing trend in ice discharge is the combination of substantially different regional, and even individual glacier, behavior that is likely the result of differences in ocean and

atmospheric forcing<sup>17,28,29</sup>. Within the past 3 years, this variability ranges from declining  $D$  in the CW due to slowing of Jakobshavn Isbræ, to variable but trendless  $D$  in the SE, to episodically increasing  $D$  in the CE due largely to Kangerdlugssuaq, to continued acceleration in the NW. Thus, rather than indicating stabilization, recent changes in GrIS discharge are the result of partially offsetting regional responses to past and current forcing. Despite this regional variability, changes in discharge and front position show a remarkably consistent relationship, with every region showing a 4–5% increase in mean discharge per km of weighted mean retreat. This indicates relative uniformity in the processes that regulate outlet glacier response to changes at the calving front and provides some constraint on future mass loss. The step-increase in discharge in the early 2000's was driven primarily by synchronous, rapid retreat in the SE and secondarily in the CE, where further regional-scale rapid retreat is unlikely due to shallowing glacier beds. The potential for another such episode of regional, rapid retreat is in the NW where retreat and discharge continue to accelerate. Finally, we expect continued episodic retreat of the large glaciers such as Jakobshavn Isbræ and Kangerdlugssuaq, that currently dominate net GrIS discharge since they are positioned on retrograde slopes<sup>22,23,29</sup>. Ultimately, predictions of future change will require improved understanding of the ice/ocean boundary and controls on glacier calving.

## Methods

We have extended the ice discharge estimates of King et al.<sup>3</sup> by two decades by integrating historical velocity data (LANDSAT 4 and 5), derived using the MIMC2 feature tracking algorithm<sup>30</sup>, with the AeroDEM digital elevation model<sup>31</sup>. We also append the extended time series, now covering an ~34-year period from 1985 to 2018, with annually resolved SAR (Synthetic Aperture Radar) velocity mosaics from ref. 4 between 1990 and 1999, which were computed mostly from wintertime observations. We use this series to assess decadal trends in ice discharge from the GrIS, and where possible, resolve the seasonal amplitude through time. We combine the dynamic ice loss component with 1-km downscaled estimates of surface mass balance (SMB) from RACMO2.3p2 over the full 1985–2018 time period<sup>15</sup>. We sum the two terms to derive more than three decades [1985–2018] of total ice mass balance that is independent of the total ice sheet mass balance derived from elevation change and gravimetry methods.

We derive ice thicknesses every 250 m along the flux gates by differencing time-varying surface elevation data, beginning with the earliest AeroDEM data through ArcticDEM<sup>32</sup>, generated by SETSM (Surface Extraction with TIN-based Search-space Minimization) algorithm<sup>33</sup> with bed topography from BedMachine v3<sup>34</sup>. We replace BedMachine v3 data with gravity inversion solutions from ref. 29 at select regions along the southeast margin, which improved bathymetry constraints for ten fjord systems using multibeam echo sounding data combined with airborne gravity data from Operation IceBridge. We combine spatially variable errors in bed topography, treated as systematic errors derived from the BedMachine v3 product, with an estimated random error of  $\pm 5$  m from surface elevation data when computing total ice thickness errors. Following ref. 5, we apply a correction based on typical velocity-thickness relationships to a subset of 39 glaciers with ice thicknesses that are too small for flowing ice, located mostly within the southeast and central east regions of the ice sheet. Using the remaining thickness data, we derive unique solutions from the best linear fit between centerline velocity and flux-gate thickness. We find that thickness increases more gradually with increasing velocity at wider flux gates. Therefore, we discretize glaciers into subgroups based on glacier width along the flux gate (Supplementary Fig. 9) rather than using a single linear fit for all glaciers and apply an adjusted ice thickness term based on the discretized solutions. This binning method improves our baseline thickness adjustments at the individual glacier scale and increases net ice sheet discharge by a time series average of  $13 \pm 1$  Gt yr<sup>-1</sup>.

We extend the 2000–2018 velocity record back in time to 1985 using LANDSAT 4 and 5, obtaining measurements for 133 of the 234 gates for the full record. These glaciers accounted for 78% of the net GrIS discharge between 2000 and 2018. Rather than assume constant flow and extrapolate the earliest available velocity data backward in time to account for incomplete coverage<sup>4</sup>, we account for the post-2000 acceleration of many glaciers by scaling the observed total annual  $D$  by the proportion of the mean net  $D$  accounted for by glaciers with observations before 2000. The mean contributions of individual glaciers to total  $D$  are calculated from their 2000–2005 period values, although results are closely similar if a 2000–2018 average is used instead. We fill missing monthly velocities using the procedure of ref. 3, where a Kalman filter is applied to each glacier time series using the glaciers' typical seasonal variation. Missing monthly data are more prevalent in wintertime months prior to when TerraSAR/TanDEM-X InSAR data first became available in 2007. We do not apply the Kalman filter for gap filling prior to 1998

due to multi-year gaps. Therefore, the temporal resolution of estimates in  $D$  varies from approximately monthly in the summers of 1985–1997, when optical data are available (including 1985–1990 and 1994/1995), to continuous monthly estimates after 1998.

Surface elevation observations, required for estimating ice thickness, are limited before 2000. The nominal dates of AeroDEM data vary spatially between 1978 and 1987, with a nominal date of 1983<sup>31</sup>, and therefore, temporal gaps range from 15 to 22 years between AeroDEM and available Advanced Spaceborne Thermal Emission and Reflection radiometer (ASTER) DEM data. To account for the uncertainty in  $D$  due to this temporal gap in ice thickness observations, we estimate  $D$  assuming the end member-cases of (1) all thickness change occurring in the first year, which maximizes the impact of thinning at the start of the period, and (2) all thinning occurring in the last year, which minimizes the impact until ~2000. This range in the timing of thinning yields an average uncertainty in  $D$  of 13 Gt yr<sup>-1</sup> during the 1985–1999 period (Fig. 1a).

We also combine velocity and ice thickness data with an extended time series of changes in calving front position at all 234 glaciers. Centerline front position data are manually digitized using optical imagery from ASTER and LANDSAT 4–8 following methods described in ref. 35, and filtered and weighted by glacier flux, when applicable, as described in ref. 3. Last, we compute net annual surface mass balance (SMB) and reference period GrIS-wide SMB using RACMO2.3p2<sup>15</sup>, and combine this term with  $D$  to derive net ice sheet mass balance for 1985–2018. Front position and discharge data from this study are publicly available<sup>36</sup>.

## Data availability

The velocity data maps and GIMP DEM are distributed through the NASA Distributed Active Archive Center at the NSIDC (<http://nsidc.org/data/measures/gimp>). Bed topography can also be accessed through the NSIDC portal at <https://nsidc.org/data/idbmg4> with supplemental topography for southeast Greenland from <https://faculty.sites.uci.edu/erignot/>. RACMO2.3p2 SMB data information can be accessed at <http://www.projects.science.uu.nl/iceclimate/models/greenland.php>. Underlying data for the main manuscript figures is included as an excel file in source data. Individual glacier time series, including monthly ice discharge, front position change, velocity, and ice thickness, are available and can be accessed at <https://doi.org/10.5061/dryad.qrf6q5cb>.

Received: 22 February 2020; Accepted: 7 May 2020;

Published online: 13 August 2020

## References

1. Shepherd, A. & IMBIE Team. Mass balance of the Greenland Ice Sheet from 1992 to 2018. *Nature* **579**, 233–239 (2020).
2. van den Broeke, M. R. et al. On the recent contribution of the Greenland ice sheet to sea level change. *Cryosphere* **10**, 1933–1946 (2016).
3. King, M. D. et al. Seasonal to decadal variability in ice discharge from the Greenland Ice Sheet. *Cryosphere* **12**, 3813–3825 (2018).
4. Mouginot, J. et al. Forty-six years of Greenland Ice Sheet mass balance from 1972 to 2018. *Proc. Natl Acad. Sci. USA* **116**, 9239–9244 (2019).
5. Mankoff, K. D. et al. Greenland Ice Sheet solid ice discharge from 1986 through 2017. *Earth Syst. Sci. Data* **11**, 769–786 (2019).
6. Carr, J. R., Stokes, C. R. & Vieli, A. Threefold increase in marine-terminating outlet glacier retreat rates across the Atlantic Arctic: 1992–2010. *Ann. Glaciol.* **58**, 1–20 (2017).
7. Bevan, S. L., Luckman, A. J. & Murray, T. Glacier dynamics over the last quarter of a century at Helheim, Kangerdlugssuaq and 14 other major Greenland outlet glaciers. *Cryosphere* **6**, 923–937 (2012).
8. Vijay, S. et al. Resolving seasonal ice velocity of 45 Greenlandic glaciers with very high temporal details. *Geophys. Res. Lett.* **46**, 1485–1495 (2019).
9. Joughin, I., Abdalati, W. & Fahnestock, M. Large fluctuations in speed on Greenland's Jakobshavn Isbræ glacier. *Nature* **432**, 609–610 (2004).
10. Khazendar, A. et al. Interruption of two decades of Jakobshavn Isbræ acceleration and thinning as regional ocean cools. *Nat. Geosci.* **12**, 277–283 (2019).
11. Joughin, I., E. Shean, D., E. Smith, B. & Floricioiu, D. A decade of variability on Jakobshavn Isbræ: Ocean temperatures pace speed through influence on mélange rigidity. *Cryosphere* **14**, 211–227 (2020).
12. Howat, I. M., Joughin, I., Tulaczyk, S. & Gogineni, S. Rapid retreat and acceleration of Helheim Glacier, east Greenland. *Geophys. Res. Lett.* **32**, L22502 (2005).
13. Howat, I. M., Joughin, I., Fahnestock, M., Smith, B. E. & Scambos, T. A. Synchronous retreat and acceleration of southeast Greenland outlet glaciers 2000–06: ice dynamics and coupling to climate. *J. Glaciol.* **54**, 646–660 (2008).
14. Brough, S., Carr, J. R., Ross, N. & Lea, J. M. Exceptional retreat of Kangerlussuaq Glacier, east Greenland, between 2016 and 2018. *Front. Earth Sci.* **7**, 1–11 (2019).

15. Noël, B., van de Berg, W. J., Lhermitte, S. & van den Broeke, M. R. Rapid ablation zone expansion amplifies north Greenland mass loss. *Sci. Adv.* **5**, 2–11 (2019).
16. Wouters, B., Bamber, J. L., Van Den Broeke, M. R., Lenaerts, J. T. M. & Sasgen, I. Limits in detecting acceleration of ice sheet mass loss due to climate variability. *Nat. Geosci.* **6**, 613–616 (2013).
17. Sasgen, I. et al. Timing and origin of recent regional ice-mass loss in Greenland. *Earth Planet. Sci. Lett.* **333–334**, 293–303 (2012).
18. van den Broeke, M. et al. Greenland Ice Sheet surface mass loss: recent developments in observation and modeling. *Curr. Clim. Chang. Reports* **3**, 345–356 (2017).
19. Nick, F. M., Vieli, A., Howat, I. M. & Joughin, I. Large-scale changes in Greenland outlet glacier dynamics triggered at the terminus. *Nat. Geosci.* **2**, 110–114 (2009).
20. Catania, G. A. et al. Geometric controls on tidewater glacier retreat in central western Greenland. *J. Geophys. Res. Earth Surf.* **123**, 2024–2038 (2018).
21. Bunce, C., Carr, J. R., Nienow, P. W., Ross, N. & Killick, R. Ice front change of marine-terminating outlet glaciers in northwest and southeast Greenland during the 21st century. *J. Glaciol.* **64**, 523–535 (2018).
22. Wood, M. et al. Ocean-induced melt triggers glacier retreat in northwest Greenland. *Geophys. Res. Lett.* **45**, 8334–8342 (2018).
23. Beckmann, J. et al. Modeling the response of Greenland outlet glaciers to global warming using a coupled flow line–plume model. *Cryosphere* **13**, 2281–2301 (2019).
24. Larsen, S. H. et al. Increased mass loss and asynchronous behavior of marine-terminating outlet glaciers at Upernavik Isstrøm, NW Greenland. *J. Geophys. Res. Earth Surf.* **121**, 241–256 (2016).
25. Veitch, S. A. & Nettles, M. Spatial and temporal variations in Greenland glacial-earthquake activity, 1993–2010. *J. Geophys. Res. Earth Surf.* **117**, F04007 (2012).
26. Weidick, A. in *Satellite Image Atlas of Glaciers of the World* (eds Williams, R. S. & Ferrigno, J.) C1–C105 (US Geological Survey, Denver, CO, 1995).
27. Howat, I. M. et al. Mass balance of Greenland’s three largest outlet glaciers, 2000–2010. *Geophys. Res. Lett.* **38**, 1–5 (2011).
28. Porter, D. F. et al. Identifying spatial variability in Greenland’s outlet glacier response to ocean heat. *Front. Earth Sci.* **6**, 1–13 (2018).
29. Millan, R. et al. Vulnerability of Southeast Greenland glaciers to warm Atlantic water from Operation IceBridge and Ocean Melting Greenland Data. *Geophys. Res. Lett.* **45**, 2688–2696 (2018).
30. Jeong, S., Howat, I. M. & Ahn, Y. Improved multiple matching method for observing glacier motion with repeat image feature tracking. *IEEE Trans. Geosci. Remote Sens.* **55**, 2431–2441 (2017).
31. Korsgaard, N. J., Nuth, C., Khan, S. A. & Kjeldsen, K. K. Digital elevation model and orthophotographs of Greenland based on aerial photographs from 1978–1987. *Sci. Data* **3**, 1–15 (2016).
32. Porter, C. et al. *ArcticDEM, V1* (Harvard Dataverse, 2018).
33. Noh, M. J. & Howat, I. M. The surface extraction from TIN based Search-space Minimization (SETSM) algorithm. *ISPRS J. Photogramm. Remote Sens.* **129**, 55–76 (2017).
34. Morlighem, M. et al. BedMachine v3: complete bed topography and ocean bathymetry mapping of Greenland from multibeam echo sounding combined with mass conservation. *Geophys. Res. Lett.* **44**, 11051–11061 (2017).
35. Walsh, K. M., Howat, I. M., Ahn, Y. & Enderlin, E. M. Changes in the marine-terminating glaciers of central east Greenland, 2000–2010. *Cryosphere* **6**, 211–220 (2012).
36. King, M. et al. *Greenland Outlet Glacier Discharge*, Ohio State University, Dataset. <https://doi.org/10.5061/dryad.qrfj6q5cb> (2020).

### Acknowledgements

This project was supported by grants 80NSSC18K1027 and NNX13AI21A from the National Aeronautics and Space Administration and a Distinguished University Fellowship from the Ohio State University. B.W. was funded by NWO VIDI grant 016.Vidi.171.063. B.P.Y.N. was funded by NWO VENI grant VI.Veni.192.019. M.R.v.d.B. and B.P.Y.N. acknowledge funding from the Netherlands Earth System Science Center (NESSC).

### Author contributions

M.D.K. and I.M.H. designed the study and analyzed main results. M.D.K. led writing of the paper. M.R.v.d.B., B.P.Y.N., S.J., and B.W. contributed data and analysis. S.G.C. and M.J.N. processed digital elevation data. A.N. worked on manual extraction of ice fronts. All authors contributed to editing and discussion of the paper.

### Competing interests

The authors declare no competing interests.

### Additional information

**Supplementary information** is available for this paper at <https://doi.org/10.1038/s43247-020-0001-2>.

**Correspondence** and requests for materials should be addressed to M.D.K.

**Peer review information** Primary handling editor: Heike Langenberg.

**Reprints and permission information** is available at <http://www.nature.com/reprints>

**Publisher’s note** Springer Nature remains neutral with regard to jurisdictional claims in published maps and institutional affiliations.



**Open Access** This article is licensed under a Creative Commons Attribution 4.0 International License, which permits use, sharing, adaptation, distribution and reproduction in any medium or format, as long as you give appropriate credit to the original author(s) and the source, provide a link to the Creative Commons license, and indicate if changes were made. The images or other third party material in this article are included in the article’s Creative Commons license, unless indicated otherwise in a credit line to the material. If material is not included in the article’s Creative Commons license and your intended use is not permitted by statutory regulation or exceeds the permitted use, you will need to obtain permission directly from the copyright holder. To view a copy of this license, visit <http://creativecommons.org/licenses/by/4.0/>.

© The Author(s) 2020